

Coherent Two-Photon LIDAR with Incoherent Light

Chung-Hyun Lee^{1,*}, Yosep Kim¹, Dong-Gil Im¹, U-Shin Kim¹, Vincenzo Tamma,² and Yoon-Ho Kim^{1,†}¹Department of Physics, Pohang University of Science and Technology (POSTECH), Pohang 37673, Korea²School of Mathematics and Physics, University of Portsmouth, Portsmouth PO1 3QL, United Kingdom (Received 29 July 2023; accepted 24 October 2023; published 28 November 2023)

Coherent light detection and ranging (LIDAR) offers exceptional sensitivity and precision in measuring the distance of remote objects by employing first-order interference. However, the ranging capability of coherent LIDAR is principally constrained by the coherence time of the light source determined by the spectral bandwidth. Here, we introduce coherent two-photon LIDAR, which eliminates the range limitation of coherent LIDAR due to the coherence time. Our scheme capitalizes on the counterintuitive phenomenon of two-photon interference of thermal light, in which the second-order interference fringe remains impervious to the short coherence time of the light source determined by the spectral bandwidth. By combining this feature with transverse two-photon interference of thermal light, we demonstrate distance ranging beyond the coherence time without relying on time-domain interference fringes. Moreover, we show that our coherent two-photon LIDAR scheme is robust to turbulence and ambient noise. This work opens up novel applications of two-photon correlation in classical light.

DOI: 10.1103/PhysRevLett.131.223602

Introduction.—Light detection and ranging (LIDAR) is an active remote sensing technology widely employed in various applications, including geospatial mapping, autonomous vehicles, and 3D imaging [1]. In commercial applications, LIDAR systems typically utilize incoherent detection, which relies on time-of-flight measurements of the reflected laser pulse to determine distance. Coherent LIDAR, operating through the interference of the reflected laser and reference laser, offers additional benefits such as ambient light suppression and enhanced sensitivity [2]. However, the coherence time, determined by the spectral bandwidth of the light source, imposes a new limitation on the maximum detection range of coherent LIDAR in addition to the laser power, which is common to both incoherent and coherent LIDAR systems [3]. When the target distance exceeds half of the longitudinal coherence length (i.e., the coherence time multiplied by the speed of light in vacuum), coherent LIDAR experiences signal quality deterioration caused by random phase noise [4]. Overcoming these limitations is a crucial step in unlocking the full potential of coherent LIDAR and advancing LIDAR technology [5].

In this Letter, we propose and demonstrate a novel concept of coherent two-photon LIDAR with incoherent light, which effectively eliminates the range restriction imposed by the spectral bandwidth of the light source. Our method significantly diverges from traditional coherent LIDAR by harnessing the counterintuitive phenomenon of two-photon interference of incoherent (thermal) light, predicated on the extraction of extremely long two-photon coherence from a short coherence light source. Notably, our scheme provides accurate and precise ranging of a remote

object situated far beyond the coherence time dictated by the spectral bandwidth of the light source. Further, our coherent two-photon LIDAR demonstrates robustness against ambient noise and atmospheric turbulence, a trait attributed to the correlation measurement and two-photon interference. Also, our coherent two-photon LIDAR with incoherent light is qualitatively different from previously reported two-photon LIDAR schemes [6,7], where the time-of-flight measurement of an optical pulse is performed via two-photon absorption/detection [6] or via Hong-Ou-Mandel-like classical interference [7–9].

Conceptual scheme.—The conceptual scheme for coherent two-photon LIDAR with incoherent thermal light is shown in Fig. 1. First, a continuous-wave (CW) thermal light source is prepared by focusing a CW laser of wavelength λ and the spectral bandwidth $\Delta\lambda$ (thus defining the

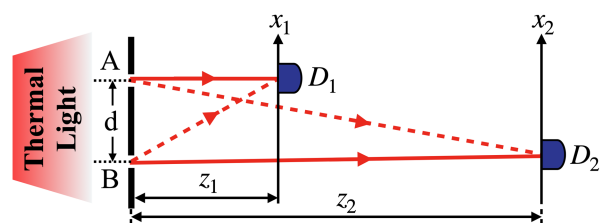


FIG. 1. Conceptual scheme of coherent two-photon LIDAR. CW thermal light of bandwidth $\Delta\lambda$ passes through a double slit whose slit separation d is larger than the transverse coherence length, so no first-order interference occurs at the detectors. D_2 registers light reflected from a remote object (not shown) and $z_2 - z_1 \gg l_c$, where $l_c \approx \lambda^2/\Delta\lambda$. We consider the intensity correlation between the signals at D_1 and D_2 .

longitudinal coherence length $l_c \approx \lambda^2/\Delta\lambda$) on a slowly rotating ground disk [10,11]. The CW thermal light is then sent through a pair of pinholes A and B separated by distance d . Detectors D_1 and D_2 are located at distances z_1 and z_2 from the double pinhole, respectively. The pinhole separation d is larger than the transverse coherence length of the thermal light, so no first-order interference is observed at the detectors.

Consider the second-order intensity correlation between the signals at detectors D_1 and D_2 . For thermal light, the second-order intensity correlation does not require quantum theory [12,13], but the quantum optical description involving probability amplitudes helps to develop a simple heuristic picture of the second-order interference effect [14]. For the scheme shown in Fig. 1, the two-photon probability amplitudes that lead to second-order interference are as follows: (i) a photon from pinhole A is detected at D_1 and a photon from pinhole B is detected at D_2 (the red solid lines in Fig. 1), and (ii) a photon from pinhole A is detected at D_2 and a photon from pinhole B is detected at D_1 (the red dotted lines in Fig. 1). In the classical regime, these two-photon probability amplitudes can be picked up by the intensity fluctuation correlation $\langle \Delta I_1 \Delta I_2 \rangle$, where intensity fluctuation of detector D_1 at position x_1 is given by $\Delta I_1 = I(x_1) - \langle I(x_1) \rangle$ and ΔI_2 is defined similarly [15–17]. The intensity fluctuation correlation $\langle \Delta I_1 \Delta I_2 \rangle$ in the far-field approximation is calculated to be

$$\begin{aligned} \langle \Delta I_1 \Delta I_2 \rangle &\propto \left| e^{ik(r_{A1}+r_{B2})} + e^{ik(r_{A2}+r_{B1})} \right|^2 \\ &\propto 1 + \cos[k(r_{A1} + r_{B2} - r_{A2} - r_{B1})], \end{aligned} \quad (1)$$

where the widths of the pinholes are assumed to be infinitesimal, and the optical path r_{A1} , for instance, is from pinhole A to D_1 . Other optical paths r_{A2} , r_{B1} , and r_{B2} are defined similarly. This leads to two-photon interference in the transverse plane x_1 and x_2 as

$$\langle \Delta I_1 \Delta I_2 \rangle \propto \cos^2 \left[\frac{\pi d}{\lambda} \left(\frac{x_1}{z_1} - \frac{x_2}{z_2} \right) \right], \quad (2)$$

where λ is the central wavelength of the thermal light. It is important to point out that, unlike first-order interference, which is range limited by the longitudinal coherence length $l_c \approx \lambda^2/\Delta\lambda$, two-photon interference of thermal light, rather counterintuitively, is completely insensitive to the coherence length $l_c \approx \lambda^2/\Delta\lambda$ [18,19].

The working principle of range-unlimited coherent two-photon LIDAR using incoherent thermal light can be derived from Eq. (2). The condition for constructive two-photon interference is given by

$$x_2 = \frac{z_2}{z_1} x_1 - m \frac{\lambda z_2}{d}, \quad (3)$$

where $m = 0, \pm 1, \pm 2, \dots$. Detector D_1 is positioned at a known distance z_1 from the double slit, and detector D_2

registers photons reflected from a remote object (not shown in the figure) with $z_2 - z_1 \gg l_c$. We can, therefore, extract an unknown distance z_2 from the slope of the two-dimensional two-photon interference fringe in the (x_1, x_2) plane with the known reference distance z_1 . It is worth pointing out that the two-photon interferometric ranging using thermal light does not require knowledge of the wavelength and that of the double pinhole.

Experimental results.—We now describe the experimental setup to demonstrate range-unlimited coherent two-photon LIDAR using thermal light. The experimental setup is shown in Fig. 2(a). A CW diode laser (CUBE, Coherent) having the central wavelength of $\lambda = 783.05$ nm and the full width at half-maximum (FWHM) bandwidth of $\Delta\lambda = 52$ pm, see Fig. 2(b), is used to generate thermal light by passing it through a rotating ground glass disk. The longitudinal coherence length of the CW diode laser is measured to be, according to the Gaussian fit to the spectral data, $l_c = (2 \ln 2/\pi)(\lambda^2/\Delta\lambda) \approx 5.2$ mm. (The corresponding coherence time is 17.3 ps.) The transverse coherence length is determined by the rotating ground disk and can be measured by the intensity autocorrelation of images obtained using a camera (CS165MU, Thorlabs). Consider an intensity value $I(x_i, y_j; t_k)$, where (x_i, y_j) is the pixel coordinate and t_k is the k th image frame recorded at the camera. The transverse intensity autocorrelation is given by

$$g^{(2)}(x_i - x_0) = \frac{\langle I(x_0)I(x_i) \rangle_{y,t}}{\langle I(x_0) \rangle_{y,t} \langle I(x_i) \rangle_{y,t}},$$

where x_0 is the horizontal center position of the images and $\langle I(x_i) \rangle_{y,t} = (1/NM) \sum_j^N \sum_k^M I(x_i, y_j; t_k)$, with N being the total number of vertical pixels per image frame and M being the total number of image frames recorded. The measured transverse spatial second-order correlation function $g^{(2)}(x_i - x_0)$ is shown in Fig. 2(c), and the thermal nature of the light source is clearly demonstrated with $g^{(2)}(0) = 1.96$. The transverse spatial coherence length is measured to be 135.7 μm at FWHM.

The thermal light is then sent through a double pinhole and immediately split into two beams with beam splitter (BS), see Fig. 2(a). The double pinhole has the pinhole separation $d = 0.5$ mm, and each pinhole has a diameter $w = 0.1$ mm. The reflected beam at BS is detected at CMOS1 at the optical path z_1 , and the transmitted beam at BS is sent to a remote object. The reflected beam from the remote object is detected at CMOS2 at the total optical path $z_2 = z'_2 + 2z_o$. At both of the CMOS cameras (CS165MU, Thorlabs), no Young-type first-order interference is observed because the transverse coherence length of the thermal light is much smaller than the pinhole separation of 0.5 mm.

The protocol for remotely estimating the object distance z_2 from the two-photon interference of thermal light beyond the coherence time is schematically shown in

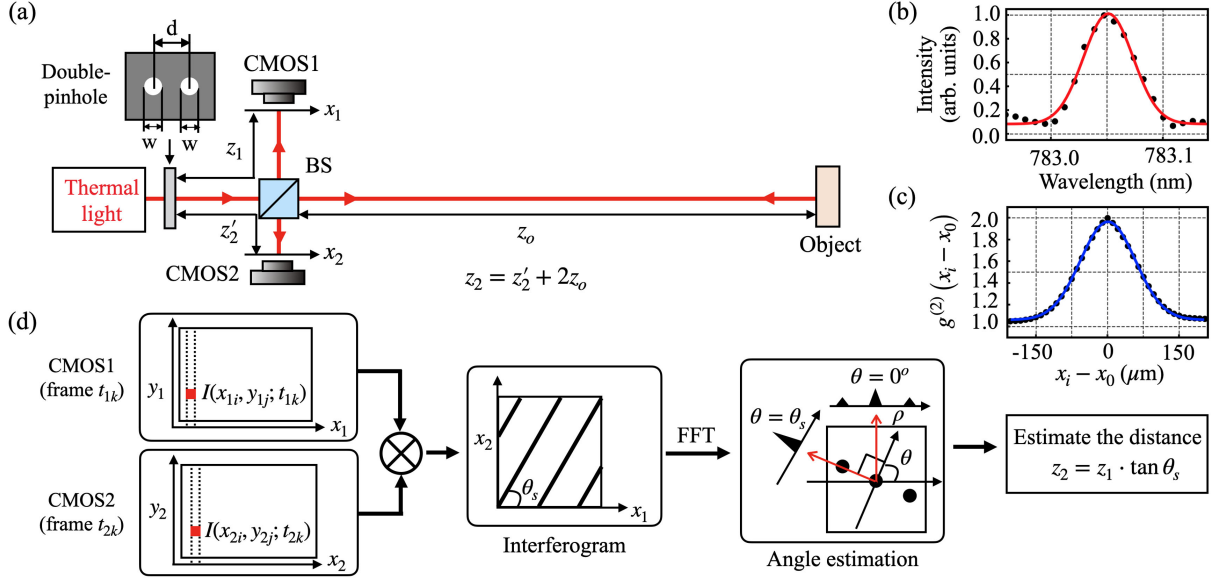


FIG. 2. (a) Schematic of the experimental setup. CMOS1 and CMOS2, respectively, are positioned at the optical paths z_1 and z_2 from the double pinhole, and $z_2 - z_1 \gg l_c$. (b) The spectrum of the diode laser. (c) The transverse spatial coherence of the thermal light. (d) The distance z_2 is calculated from the angle θ_s of the two-photon interferogram.

Fig. 2(d). First, two-photon interference is observed in the intensity fluctuation correlation between CMOS1 [with (x_1, y_1) pixel coordinate] and CMOS2 [with (x_2, y_2) pixel coordinate]. Note that CMOS1 distance z_1 is measured locally, and we aim to measure the object distance $z_2 = z_2' + 2z_0$. We also emphasize that, to clearly demonstrate coherent two-photon LIDAR beyond the coherence time, the condition $z_2 - z_1 \gg l_c$, should be strictly satisfied. The intensity fluctuation correlation between CMOS1 and CMOS2 is obtained as follows:

$$\begin{aligned} \langle \Delta I_1 \Delta I_2 \rangle_{y,t} &= \frac{1}{NM} \sum_j^N \sum_k^M \Delta I(x_{1i}, y_{1j}; t_{1k}) \Delta I(x_{2i}, y_{2j}; t_{2k}), \quad (4) \end{aligned}$$

where, for instance, the intensity fluctuation at pixels on CMOS1 is defined as $\Delta I(x_{1i}, y_{1j}; t_{1k}) = I(x_{1i}, y_{1j}; t_{1k}) - \langle I(x_{1i}) \rangle_{y,t}$. In the experiment, $N = 1,080$ is the number of vertical pixels per image, and M is the total number of the frames recorded (typically M on the order of 10^3).

To optimize the value of the fluctuation correlation $\langle \Delta I_1 \Delta I_2 \rangle_{y,t}$ in Eq. (4), we adjust the vertical offset ($y_{2j} = y_{1j} + \Delta y$) and the temporal offset ($t_{2k} = t_{1k} + \Delta t$) as follows. Consider the pair of one-dimensional data for the vertical pixels $\langle I(y_{1j}) \rangle_{x,t}$ and $\langle I(y_{2j}) \rangle_{x,t}$, and the pair of one-dimensional for the frame numbers $\langle I(t_{1k}) \rangle_{x,y}$ and $\langle I(t_{2k}) \rangle_{x,y}$. The vertical pixel offset and the temporal offset, respectively, are identified by maximizing the cross-correlation between $\langle I(y_{1j}) \rangle_{x,t}$ and $\langle I(y_{2j}) \rangle_{x,t}$, and between $\langle I(t_{1k}) \rangle_{x,y}$ and $\langle I(t_{2k}) \rangle_{x,y}$. We utilized the fast-Fourier

transform (FFT) to calculate the cross-correlation fast and efficiently [20]. Once the offset values Δy and Δt are identified, the intensity fluctuation correlation in Eq. (4) is maximized using the offset values, $\langle \Delta I_1 \Delta I_2 \rangle_{y,t} = (1/NM) \sum_{j_1}^N \sum_{k_1}^M \Delta I(x_{1i}, y_{1j_1}; t_{1k_1}) \Delta I(x_{2i}, y_{1j_1} + \Delta y; t_{1k_1} + \Delta t)$. We note that the vertical offset correction is not always necessary, and a summation over the vertical pixels is usually sufficient. There are, however, situations in which such corrections may be useful. Refer to the Supplemental Material [21] for details.

The resulting experimental data, two-photon interference of thermal light revealed in the intensity fluctuation correlation in the (x_1, x_2) plane as a function of varying object distance z_2 with $z_2 - z_1 \gg l_c$, are shown in Fig. 3(a). As expected from Eq. (3), the interferometric fringe slope becomes steeper with z_2 . The fringe slope can be extracted by FFT followed by the radon transform. The Fourier transform of the fringe pattern has three peaks at the spatial frequencies $[(2\pi d/\lambda z_1), -(2\pi d/\lambda z_2)]$, $(0,0)$, and $[-(2\pi d/\lambda z_1), (2\pi d/\lambda z_2)]$ as shown in Fig. 3(b). FFT converts a difficult global detection problem in the image domain into a more easily solved local peak detection problem in the spatial frequency domain. Note that the slopes of the interference fringes and the Fourier peaks are perpendicular to each other. The radon transformation of a two-dimensional Fourier spectrum in Fig. 3(b) is obtained by projecting the pixel value at an angle θ with respect to the abscissa and is described by the relation [22,23]

$$R(\rho, \theta) = \int_{-\infty}^{\infty} f(x, y) \delta(\rho - x \cos \theta - y \sin \theta) dx dy, \quad (5)$$

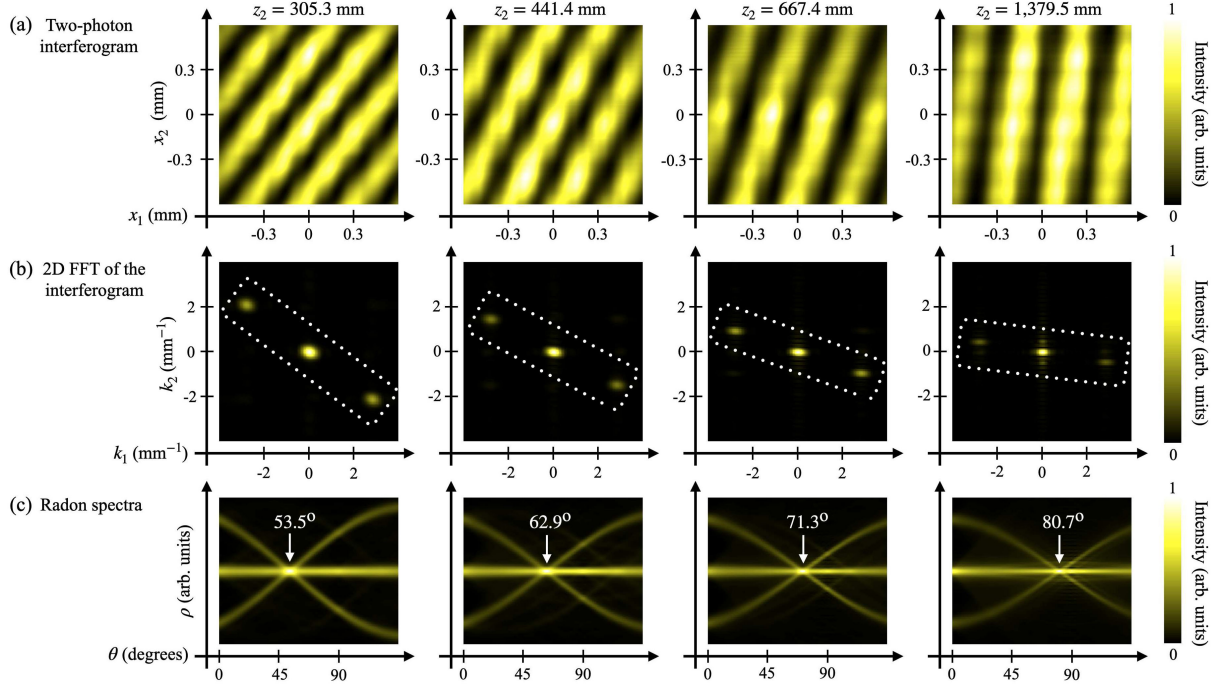


FIG. 3. Experimental data. The reference distance $z_1 = 225.9 \pm 0.8$ mm. (a) Two-photon interferogram revealed in $\langle \Delta I_1 \Delta I_2 \rangle$ for different object distances z_2 . (b) Two-dimensional FFT of the interferogram reveals three distinct peaks aligned on a straight line. (c) Radon spectra of the 2D FFT reveals the fringe angle θ_s . The remote distance z_2 is estimated from $z_2 = z_1 \tan \theta_s$.

where δ is the Kronecker delta function and ρ is the distance from the origin to the perpendicular offset of the line $y = x \tan \theta$. As a result, two sinusoids, the radon transforms of off-center Fourier peaks in the spatial Fourier spectrum, cross each other at a certain angle θ_s . Figure 3(c) shows the radon spectra of the corresponding two-dimensional Fourier spectra. Finally, the distance $z_2 = z_2' + 2z_0$, where z_0 is the distance of the remote object, is estimated from $z_2 = z_1 \tan \theta_s$.

Note that the accuracy of estimating the remote distance z_2 is also dependent on how accurately the reference distance z_1 is measured. Although z_1 may be measured locally, we exploit the two-photon interference effect due to the double pinhole observed on CMOS1 to estimate the reference distance z_1 . In the far zone, taking into consideration of the finite pinhole size, the second-order interference-diffraction pattern is given by [15], $\langle \Delta I_1(x_i) \Delta I_1(x_j) \rangle_{y,t} \propto \sin^2(\pi w \Delta x_1 / \lambda z_1) \cos^2(\pi d \Delta x_1 / \lambda z_1)$, where $\Delta x_1 = x_i - x_j$ is the distance between pixels x_i and x_j on the CMOS1. The experimentally obtained one-dimensional interference-diffraction pattern $\langle \Delta I_1(x_i) \Delta I_1(x_0) \rangle_{y,t}$, where x_0 is the horizontal center position of CMOS1, can be used to accurately estimate the reference distance z_1 .

Discussion.—For coherent LIDAR, light detection must inherently be limited to a single optical mode as interference between the reference and the reflected light is measured. Therefore, the optical mode distortion caused by atmospheric turbulence results in severe degradation of

detected optical power, making coherent LIDAR extremely susceptible to atmospheric turbulence [24,25]. For the two-photon coherent LIDAR presented in this work, the scheme is inherently robust to atmospheric turbulence [26]. Consider arbitrary phase fluctuation $e^{i\phi'_A}$ and $e^{i\phi'_B}$ affecting the optical paths between the double pinhole and the remote object in the conceptual schematic shown in Fig. 1. The phase factors $e^{i\phi'_A}$ and $e^{i\phi'_B}$ refer to, respectively, time-dependent phase fluctuation introduced to the optical paths between pinhole A and pinhole B to the remote object. The intensity fluctuation correlation in Eq. (1) is then revised to

$$\begin{aligned} \langle \Delta I_1 \Delta I_2 \rangle &\propto |e^{ik(r_{A1}+r_{B2})+i\phi'_B} + e^{ik(r_{A2}+r_{B1})+i\phi'_A}|^2 \\ &\propto 1 + \cos[k(r_{A1} + r_{B2} - r_{A2} - r_{B1}) + \Delta\phi'], \end{aligned}$$

where $\Delta\phi' = \phi'_B - \phi'_A$ is the relative phase difference. As the atmospheric coherence length (i.e., the Fried parameter r_0 , which is defined as the diameter of a circular area over which the rms wavefront aberration due to the transmission through the atmosphere is equal to 1 rad) is significantly larger than the separation distance between the pinholes, our scheme is inherently robust to atmospheric turbulence [27].

Moreover, our two-photon coherent LIDAR scheme is robust to ambient light noise [28]. Consider optical intensity recorded at D_2 , which includes the optical path for the remote object: the signal intensity is I_s and the ambient noise contribution is I_n . The intensity fluctuation

correlation can be written as $\langle \Delta I_1 \Delta I_2 \rangle = \langle \Delta I_1 \Delta (I_s + I_n) \rangle = \langle \Delta I_1 \Delta I_s \rangle + \langle \Delta I_1 \Delta I_n \rangle$. Since the fluctuation of the ambient light ΔI_n is independent of ΔI_1 , the second term vanishes and does not affect the result. Hence, our two-photon coherent LIDAR scheme is also robust to ambient light noise.

Analysis.—Although our coherent two-photon LIDAR eliminates the range limitation of coherent LIDAR due to the coherence time of the light, the object distance z_2 is estimated from the measured slope $\tan \theta_s$ of the interferogram in the (x_1, x_2) plane via $\tan \theta_s = z_2/z_1$. Since the two-photon interferogram is obtained from intensity fluctuation correlation between pixels at two detectors, see Eq. (4), the slope measurement is limited by the number of horizontal pixels. A simple solution is to use larger sensors or to introduce a telescope system with a magnification factor of \mathcal{M} in front of CMOS2 in Fig. 2, modifying Eq. (2) to $\cos^2\{(\pi d/\lambda)[(x_1/z_1) - (\mathcal{M}x_2/z_2)]\}$. Consequently, the slope of the interferogram is reduced to $\tan \theta_s = z_2/(\mathcal{M}z_1)$, allowing us to extend the measurement range by a factor of \mathcal{M} .

We now analyze the sensitivity of our scheme by calculating the Cramér-Rao bound. Considering Eq. (2), we adopt a sinusoidal signal model $S(n_1, n_2) = \bar{I}^2(1 + V \cos[\omega_1 n_1 - \omega_2 n_2])$, where \bar{I} is the mean pixel value, V is the two-photon interference visibility, and n_1 (n_2) is the pixel number in the x_1 (x_2) direction. The spatial frequency of the two-photon interference in the x_1 (x_2) direction is ω_1 (ω_2). By considering the Poisson random variable approach [29], the Cramér-Rao bound for the standard deviation σ_{z_2} of the z_2 measurement is approximately found to be $(\sigma_{z_2})^2 \geq [3/(1 - \sqrt{1 - V^2})](z_2/\bar{I}\omega_2 N_H^2)^2$, where N_H is the number of horizontal pixels; see the Supplemental Material [21] for detailed calculations for the Fisher information. This result clearly shows how certain experimental parameters affect the distance measurement accuracy in our scheme.

In summary, we have proposed and experimentally demonstrated coherent two-photon LIDAR, eliminating the range limitation of coherent LIDAR due to the coherence time of the light source defined by the spectral bandwidth. By exploiting the two-photon coherence and two-photon interferometry of thermal light, in which the second-order interference fringe remains impervious to the short coherence time of the light source, we have demonstrated distance ranging beyond the coherence time without relying on time-domain interference fringes. Furthermore, we have shown that our coherent two-photon LIDAR scheme is robust to atmospheric turbulence and ambient noise. We anticipate that this work will open up various novel applications of two-photon correlation in

classical light and quantum-inspired applications of classical light.

This work was supported in part by the National Research Foundation of Korea (RS-2023-00208500) and the Ministry of Science and ICT of Korea under the Information Technology Research Center support program (IITP-2023-2020-0-01606 and IITP-2022-RS-2022-00164799). V.T. acknowledges support from the Air Force Office of Scientific Research (FA8655-23-1-7046).

*highrhee@gmail.com

†yoonho72@gmail.com

- [1] X. Wang, H. Pan, K. Guo, X. Yang, and S. Luo, *IOP Conf. Ser.* **502**, 012008 (2020).
- [2] C. S. Sambridge, J. T. Spollard, A. J. Sutton, K. McKenzie, and L. E. Roberts, *Opt. Express* **29**, 25945 (2021).
- [3] C. Pang, Q. Zhang, Z. Li, and G. Wu, *Sensors* **21**, 2341 (2021).
- [4] M. M. Bayer, X. Li, G. N. Guentchev, R. Torun, J. E. Velazco, and O. Boyraz, *Opt. Express* **29**, 42343 (2021).
- [5] S. Royo and M. Ballesta-Garcia, *Appl. Sci.* **9**, 4093 (2019).
- [6] H. Wright, J. Sun, D. McKendrick, N. Weston, and D. T. Reid, *Opt. Express* **29**, 37037 (2021).
- [7] R. Murray and A. Lyons, *Opt. Express* **30**, 27164 (2022).
- [8] C. K. Hong, Z. Y. Ou, and L. Mandel, *Phys. Rev. Lett.* **59**, 2044 (1987).
- [9] Y.-S. Kim, O. Slattery, P. S. Kuo, and X. Tang, *Phys. Rev. A* **87**, 063843 (2013).
- [10] Y.-W. Cho, H.-T. Lim, Y.-S. Ra, and Y.-H. Kim, *New J. Phys.* **12**, 023036 (2010).
- [11] J. E. Oh, Y.-W. Cho, G. Scarcelli, and Y.-H. Kim, *Opt. Lett.* **38**, 682 (2013).
- [12] R. Hanbury-Brown and R. Q. Twiss, *Nature (London)* **177**, 27 (1956).
- [13] B. L. Morgan and L. Mandel, *Phys. Rev. Lett.* **16**, 1012 (1966).
- [14] U. Fano, *Am. J. Phys.* **29**, 539 (1961).
- [15] G. Scarcelli, A. Valencia, and Y. Shih, *Europhys. Lett.* **68**, 618 (2004).
- [16] G. Scarcelli, V. Berardi, and Y. Shih, *Appl. Phys. Lett.* **88**, 061106 (2006).
- [17] F. V. Pepe, G. Scala, G. Chilleri, D. Triggiani, Y.-H. Kim, and V. Tamma, *Eur. Phys. J. Plus* **137**, 647 (2022).
- [18] Y. S. Ihn, Y. Kim, V. Tamma, and Y.-H. Kim, *Phys. Rev. Lett.* **119**, 263603 (2017).
- [19] G.-H. Lee, D.-G. Im, Y. Kim, U.-S. Kim, and Y.-H. Kim, *Opt. Lett.* **45**, 6748 (2020).
- [20] D. Lyon, *J. Object Technol.* **9**, 15 (2010).
- [21] See Supplemental Material at <http://link.aps.org/supplemental/10.1103/PhysRevLett.131.223602> for the explanation on the vertical pixel offset correction, and the

- detailed theoretical analysis on the measurement range and resolution.
- [22] T. A. Ramirez-delreal, M. Mora-Gonzalez, F.J. Casillas-Rod-Rodriguez, J. Munoz-Maciel, and M. A. Paz, *Opt. Express* **25**, 7150 (2017).
- [23] S. Dongfeng, H. Jian, M. Wenwen, Y. Kaixin, S. Baoqing, W. Yingjian, Y. Kee, X. Chenbo, L. Dong, and Z. Wenyue, *Opt. Express* **27**, 14594 (2019).
- [24] A. E. Siegman, *Appl. Opt.* **5**, 1588 (1966).
- [25] K. P. Chan, D. K. Killinger, and N. Sugimoto, *Appl. Opt.* **30**, 2617 (1991).
- [26] T. A. Smith and Y. Shih, *Phys. Rev. Lett.* **120**, 063606 (2018).
- [27] M. Li, P. Zhang, and J. Han, *Appl. Sci.* **12**, 2980 (2022).
- [28] J. Zhu, X. Chen, P. Huang, and G. Zeng, *Appl. Opt.* **51**, 4885 (2012).
- [29] C. Li and Y. Zhu, *Appl. Opt.* **56**, 6867 (2017).